Holo-Hilbert Spectral-based Removal of Gamma-Band Noise from Simultaneous EEG-fMRI Recordings

Narges Moradi[1,2], Pierre LeVan[2-4], Burak Akin[4,5], Bradley G. Goodyear[2], and Roberto C. Sotero[2]
[1]Biomedical Engineering Graduate Program, University of Calgary, Calgary, AB, Canada
[2]Department of Radiology and Hotchkiss Brain Institute, University of Calgary, Calgary, AB, Canada
[3]Alberta Children's Hospital Research Institute and Departments of Paediatrics, University of Calgary, Calgary, Canada,
[4]Department of Radiology, Medical Physics, Medical Center, University of Freiburg, Faculty of Medicine, Germany
[5]Section on Functional Imaging Methods, NIMH, NIH, Bethesda, MD, USA

Simultaneous EEG-fMRI is a growing and promising field, as it has great potential to further our understanding of the spatiotemporal dynamics of brain function in health and disease. In particular, there is much interest in understanding the fMRI correlates of brain activity in the gamma band (30–100 Hz), as these frequencies are thought to be associated with cognitive processes involving perception, attention and memory, as well as with disorders such as schizophrenia and autism. However, progress in this area has been limited due to the MR-induced artifacts in EEG recordings, which seem to be more problematic for gamma frequencies. This paper presents a method of MR-induced noise removal from the gamma band of EEG that is based on Holo-Hilbert spectral analysis (HHSA), but with a new implementation strategy. HHSA uses a nested empirical mode decomposition (EMD) to identify amplitude and frequency modulations (AM and FM, respectively). Instead of including all FM components, our method examines only gamma-band FM and AM components, removes components with very low power based on the power-instantaneous frequency spectrum, and subsequently reconstructs the denoised gamma-band signal from the remaining components. Simulations demonstrate that our proposed method effectively reduces artifacts while preserving the original signal.

***Index Terms*—Amplitude-modulated component, EEG, Empirical Mode Decomposition (EMD), frequency-modulated component, Gamma-band denoising, Holo-Hilbert spectral analysis (HHS), Simultaneous EEG and fMRI recording.**

I. Introduction

Electroencephalography (EEG) is a widely used technique that records electrical activity of the brain non-invasively with high temporal resolution (on the order of milliseconds), but low spatial resolution (on the order of centimeters) [1, 2]. On the other hand, functional magnetic resonance imaging (fMRI) based on the hemodynamic blood-oxygenation-level-dependent (BOLD) response localizes brain activity with high spatial resolution (on the order of millimetres), but low temporal resolution (typically 2–3 seconds) [1, 3]. Fortunately, BOLD fMRI and EEG can be collected simultaneously to permit both high spatial and temporal resolution, which improves our ability to better understand the coupling that exists between the brain's electrical activity and hemodynamic responses (i.e., neurovascular coupling) [4–8].

It has been demonstrated that the BOLD signal is associated with neuronal synchronization across a number of EEG frequency bands. The powers of the alpha (8–12 Hz) and beta (12-30 Hz) bands correlate negatively with BOLD signal magnitude, while gamma band ($>$ 30 Hz) power correlates positively with BOLD signal magnitude [9–11]. It is believed that gamma activity is most directly associated with neurovascular coupling [11–19], and some studies have shown that gamma band frequencies are the carrier frequencies associated with the temporal synchronization of intrinsic BOLD fluctuations within resting-state functional networks [11, 16, 20, 21]. Thus, the gamma band is of utmost importance in the analysis of EEG-fMRI data.

EEG simultaneously recorded during fMRI contains artifacts that cannot be simply filtered [9, 22–24]. These artifacts are primarily due to electric noise induced by the on and off switching of the magnetic field gradients. The shape and amplitude of artifacts vary depending on the EEG electrode's location, head motion, and the positioning of the leads and connectors. In addition, electromyographic (EMG) recordings of muscle contractions recorded as part of the EEG acquisition contain artifacts over a wide frequency range and are maximum at frequencies exceeding 30 Hz, which is within the gamma band [9, 22, 25]. Several noise removal methods have been proposed, including those that use Kalman filtering [26], the wavelet transform [27], blind source separation [28], principal component analysis (PCA) [28], and independent component analysis (ICA) [9, 29]. Most methods have concentrated on improving EEG signals at low frequencies ($<$ 30 Hz) [25, 30–32], but it has been shown that these denoising strategies are inadequate for the gamma band [9]. Therefore, a noise removal method for the gamma band is sorely needed. Of note, the majority of methods to date are limited to the analysis of stationary and linear signals, and require a priori or a posteriori knowledge of the underlying physiology. The latter places restrictions on automated methods.

Here, a new method is presented based on the recently introduced Holo-Hilbert spectral-based analysis (HHSA) technique [33], which consists of the Hilbert-Huang transform (HHT) [34] and the nested application of empirical mode decomposition (EMD) [35]. EMD is a data-driven method for

Corresponding authors: N. Moradi (narges.moradi1@ucalgary.ca) and R. C. Sotero (roberto.soterodiaz@ucalgary.ca)
3330 Hospital Drive NW, HSC Building, Calgary, AB, T2N 4N1, Canada

the analysis of nonlinear and non-stationary data, which makes it suitable for EEG signals [35, 36].

HHSA constructs a multidimensional power spectrum that accommodates all possible temporal properties and interactions within a signal: additive and multiplicative, intra-mode and inter-mode, stationary and nonstationary, linear and nonlinear interactions. HHSA identifies the amplitude modulation (AM) and frequency modulation (FM) within a signal based on the constructed power spectrum. According to this method, the signal of interest is first decomposed into intrinsic mode functions (IMFs) using the EMD method, known as the first layer. Then, the amplitude envelope of each of the IMFs is decomposed into a set of amplitude modulated IMFs (IMFs^{AM}), constituting the second layer. Although HHSA can go through multiple iterations until the amplitude functions bear no more cyclic characteristics in the envelopes, in practice only two iterations are performed [6, 33, 35, 37–39].

The HHSA method has been used in a number of EEG applications, including the examination of oscillatory brain activity and interactions amongst EEG frequency bands (alpha and beta bands) [6], the study of human visual system processing [37], and the derivation of time-frequency spectrum matrices to characterize sleep stages [39]. However, previous studies have not applied the second layer of EMD to the FM components of IMFs computed by the first layer; the AM frequency represents the slow-changing envelope of inter-mode frequency variations and can be used to analyze inter-mode interactions [6]. We show that applying the second layer of the EMD method to the FM components of the signal, rather than the AM components, augments the capability of HHSA to analyze intra-mode nonlinearity.

In the proposed method, the EEG signal is first decomposed into IMFs. These IMFs are combined to roughly correspond to the known EEG bands (e.g., gamma, beta) [4]. A second layer of decomposition is then applied to the AM and FM components of the gamma band to compute the gamma IMFs^{AM} and frequency-modulated IMFs (IMFs^{FM}), respectively. Analogous to AM frequency identification of the HHSA method, the carrier frequency of a signal is where power is significant and high in the power-instantaneous frequency spectrum [6, 33]. Therefore, IMFs^{AM} and IMFs^{FM} with frequencies of low power can be considered as a noise. Accordingly, the power spectrums of all of the IMFs^{AM} and IMFs^{FM} are used to identify and remove noise IMFs from the AM and FM components of the signal, respectively.

Another difference between the proposed method and the HHSA method is how the signal's AM and FM components are computed. In the HHSA method, a signal is constructed based on the FM and AM frequencies with the significant and high energy density; however, in the proposed method, the signal is constructed by integrating the remaining IMFs^{AM} and IMFs^{FM} after removing the low power IMFs^{AM} and IMFs^{FM}. Our method enhances the determination of nonlinear interactions within the signal, by providing frequency-domain information on the signal's AM and FM components. With these theorized improvements, we hypothesize that our proposed method generates more accurate and less noisy gamma-band signals than the HHSA method.

II. Methods

A. EEG data acquisition

Resting-state EEG data were recorded using a 256-channel MR-compatible EEG system (Geodesic EEG System 400, Electrical Geodesic, Inc., Eugene, OR) with a 1000 Hz sampling rate [40]. Additional ECG leads were positioned on the chest of the subject. EEG was recorded simultaneously with fMRI, and all channels were referenced to the vertex electrode, Cz. The cap diameter was adjusted to each subject before the recording. Each channel was connected to the scalp through a hypoallergenic sponge soaked in a saline solution of Potassium Chloride (KCl) and detergent. The signals were downsampled to 200 Hz, and the gradient and ballistocardiographic artifacts were removed using the methods described in [41, 42].

B. Data simulation

The background activity of the brain was modelled using 1/f-activity (or pink noise), and sensor noise was modelled at the channel level as additive white gaussian noise. To simulate the EEG's gamma band, white gaussian and pink noise were both filtered between 30 and 80 Hz. The filtered noises were then added to a 30-Hz sinusoidal signal and a combination of three 30-Hz, 60-Hz and 75-Hz sinusoidal signals to yield a SNR of ≈ 2 dB [43, 44]. The duration of the simulated signals was 50 s and the sampling rate was 200 Hz.

C. Denoising EEG signals using the proposed method

To denoise the gamma band using the proposed approach, the following steps were followed [33]:

1) The EEG signal was first decomposed into its IMFs using the EMD method [15]. The obtained IMFs roughly correspond to the known EEG bands [4], but if there was a case where several IMFs lie within the same band, they were added to obtain only one component per band. The main goal of this paper is denoising the gamma band; thus, the proposed method is applied only to the gamma band, which is denoted by γ. The gamma band signal can be written in terms of its AM and FM components as:

$$\gamma(t) = \sum_{j=1}^{N} \text{IMF}_j(t) = \text{Re} \sum_{j=1}^{N} \overbrace{A_j(t)}^{\text{AM}} * \overbrace{\mathrm{e}^{\mathrm{i} \int \omega_j(\tau) d\tau}}^{\text{FM}} \quad (1)$$

This equation corresponds to the first layer of the HHSA method, where N is the number of points in the time series, $A_j(t)$ are the instantaneous amplitudes, and $\omega_j(t)$ are the instantaneous frequencies.

2) To extract $A_j(t)$, the absolute value of $\gamma(t)$ is used to construct the upper envelope function by a natural spline function through all the maxima.

3) The envelopes $A_j(t)$ are decomposed into a set of amplitude-modulated (AM) IMFs using the EMD method, denoted as IMF^{AM}:

$$A_j(t) = \sum_{k=1}^{L} \text{IMF}_k^{\text{AM}}(t) = \text{Re} \sum_{k=1}^{L} A_{jk}(t) * \mathrm{e}^{\mathrm{i} \int \Omega_k(\tau) d\tau} \quad (2)$$

4) The instantaneous frequencies Ω_k of IMF^{AM} are then

calculated using the Hilbert transform.
5) A three-dimensional HHSA spectrum (consisting of ω, Ω, and $P(\omega, \Omega)$) is constructed by incorporating the instantaneous power, $P(\omega, \Omega)$, with the instantaneous AM frequencies of IMF^{AM} (Ω) and the instantaneous FM frequencies (ω across all time points for the gamma band signal.
6) According to the HHSA method [33], the carrier-wave and envelope-modulation frequencies (ω, Ω) are identified based on the power density in the HHSA spectrum. The prominent modulating frequencies of the signal are where the power is high and significant and are determined by averaging over the frequencies of high significant powers [33]. With computed ω and Ω, the denoised signal is constructed using Eq. (1).
The steps presented above only deal with denoising of the amplitude of the gamma band. However, a similar approach can be implemented to eliminate noise present in the FM components of the signal. According to the proposed method, the 6th step is skipped. Thus, after step 5, artifact removal analysis is performed based on the proposed method as follows:
5) $\rightarrow$ 7) A 2D power spectrum is computed based on the instantaneous power $P(\Omega)$ and frequencies, Ω, across all IMFs^{AM}.
8) The AM component of the signal is refined based on the HHSA spectrum and its 2D power spectrum. IMFs^{AM}, or part of an IMF^{AM}, of specific frequency bands are removed according to the HHSA and 2D power spectrum where power is not around its peak.
9) The FM component of the gamma band signal is computed using the Hilbert transform.
10) The FM component, which is represented in Eq. (1) as $\mathrm{e}^{\mathrm{i}\int \omega_j(\tau)d\tau}$, is decomposed into a set of frequency-modulated IMFs with instantaneous carrier-wave frequencies $\Omega_k(\tau)$ using the EMD-based method, denoted as IMF^{FM}.

$$\mathrm{e}^{\mathrm{i}\int \omega_j(\tau)d\tau} = \sum_{k=1}^{L} \mathrm{IMF}_k^{\mathrm{FM}}(t) = \mathrm{Re}\sum_{k=1}^{L} \mathrm{e}^{\mathrm{i}\int \nu_k(\tau)d\tau} \tag{3}$$

11) The instantaneous frequencies ν_k of IMF^{FM} are then calculated using the Hilbert Transform.
12) A 2D power spectrum of the FM component of the signal is computed based on the instantaneous power, $P(\nu)$, and frequencies, ν, of all IMFs^{FM}.
13) To denoise the FM part of the signal, IMFs^{FM}, or part of an IMF^{FM}, that does not contain frequencies with high power are removed.
14) Denoised AM and FM components are constructed by summing up the remaining IMFs^{FM} and IMFs^{AM}.
After processing both the AM and FM components of the signal, as shown in Eqs. (2) and (3), the integration of both the denoised AM and FM parts ($A_j(t)_R$ and $(\mathrm{e}^{\mathrm{i}\int \omega_j(\tau)d\tau})_R$ respectively), constructs the noise-reduced gamma signal (γ_R) as in Eq. (4). Here, R means noise-reduced.

$$\gamma_R(t) = \mathrm{Re}\sum_{j=1}^{N} A_j(t)_R * \left(\mathrm{e}^{\mathrm{i}\int \omega_j(\tau)d\tau}\right)_R \tag{4}$$

The HHSA method and our proposed method were applied to the simu¬lated datasets. A flowchart representing the overview of applying the proposed approach to denoise the gamma band signal is shown in Fig. 1.

As mentioned above, when an IMF contains desired frequencies with high energy and undesired frequencies with low energy, only a part of an IMF can be removed. These types of IMFs^{FM} and IMFs^{AM} can be identified by their power spectrum. Part of an IMF is removed by zeroing all frequencies other than the frequency range of interest. This usually happens in the IMFs corresponding to high frequencies in both the AM and FM spectrums. It should also be stressed here that for denoising the FM component of a signal, two cases are possible in the FM power spectrum: 1) a single peak and 2) mode-mixing or multiple peaks. When a signal contains components of close frequencies with almost the same amplitude, there might be more than one frequency in some of its IMFs after decomposition, which is typical [45, 46]. In the single-peak case, IMFs^{FM} with frequencies in the peak range of the FM-power spectrum are kept, and IMFs^{FM} that do not have high power are removed from the FM part of the signal. In the multiple-peak case, IMFs^{FM} with very low powers are simply removed, and so IMFs^{FM} over a broader range of frequencies are maintained and powers are comparable to the single-peak case. This is because IMFs^{FM} with not very low power might be created by frequency modulation in the original signal. The frequency range of the frequency-modulated signal varies between above and below the carrier frequency, depending on the maximum modulating frequency in the signal. By including more IMFs^{FM} in the FM part of the signal comprised of more than one frequency, losing part of the original signal and its information is prevented. To investigate the similarity between the pure signal (simulated signal before adding noise) and the denoised signal computed by the HHSA method and the proposed approach, we computed Mutual Information (MI) [47] using Neuroscience Information Theory Toolbox (https://github.com/nmtimme/Neuroscience-Information-Theory-Toolbox).

III. Results

The simulated pure and noisy gamma-band signals and their frequency spectra are shown in Fig. 2A–2F for simulated signals consisting of a single frequency of 30 Hz (*s-signal1*), and in Fig. 3A–3F for simulated signals containing 30 Hz, 60 Hz and 75 Hz (*s-signal2*). After computing the upper envelopes of the noisy signals, Figs. 2G and 3G, they are further decomposed into sets of IMFs^{AM} using an EMD-based method, ICEEMDAN, with 300 ensembles and a level of noise of 0.2 [36].

According to the 2D power spectrum and the HHSA spectrum of the upper envelope, the envelope-modulation frequencies are less than ≈17–20 Hz for *s-signal1* (see Fig. 4A–4C) and between 20 to 35–37 Hz for *s-signal2* (see Fig. 5A–5C). Thus, IMFs^{AM} with frequencies other than these frequency ranges are removed. Accordingly, to denoise the AM component of *s-signal1*, IMF^{AM}1 and IMF^{AM}10 to IMF^{AM}12 were removed, and frequencies higher than 20 Hz in IMF^{AM}2 were also zeroed. IMF^{AM}3 to IMF^{AM}12 were excluded based on the power spectra shown in Fig. 5 for denoising the AM

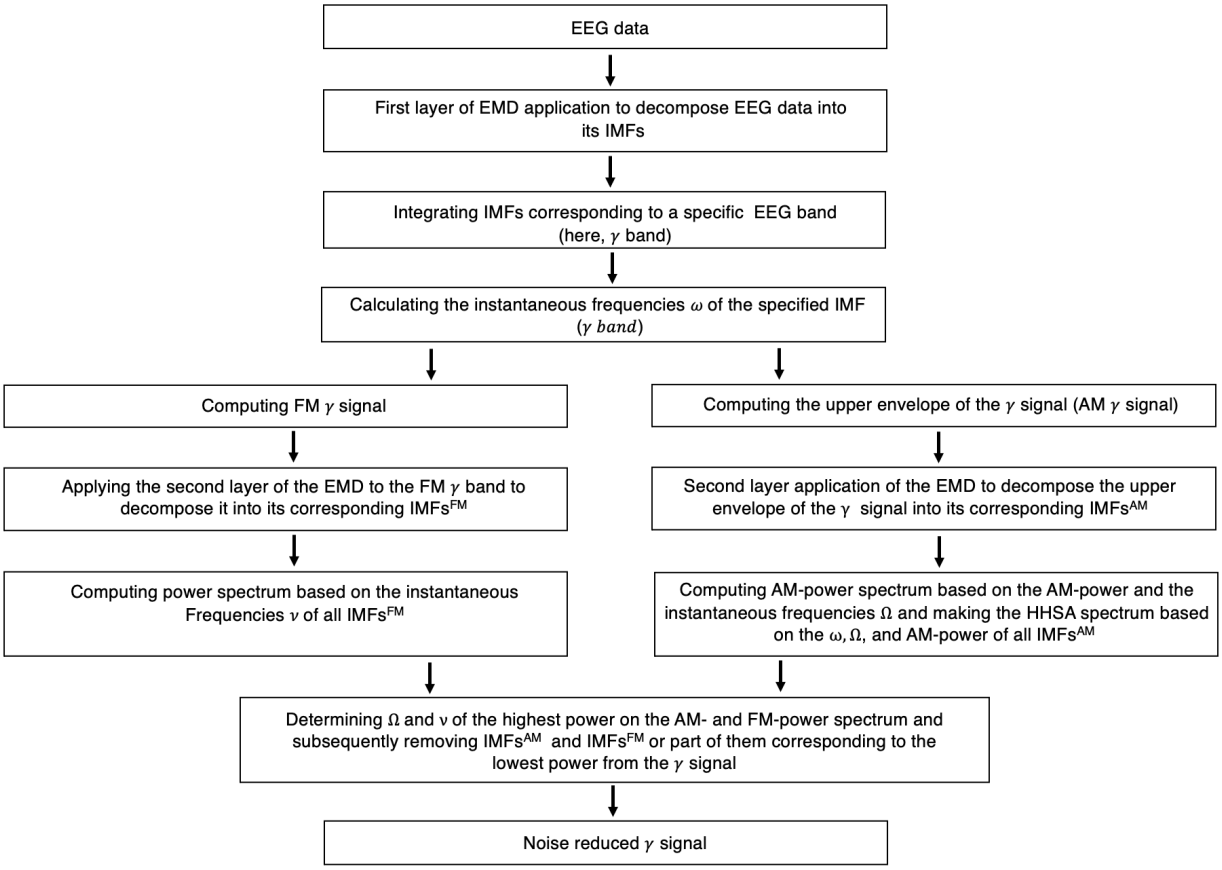

Fig. 1: Signal-processing flowchart of the proposed approach.

component of *s-signal2*. Furthermore, since white noise is a wide-band signal without modulation, it has a low modulation frequency of ≈ 0 Hz. Thus, IMFs^{AM} with a frequency lower than 0.1 Hz were also removed for both simulated signals [6].

To denoise the FM part of *s-signal1*, according to the power spectrum illustrated in Fig. 6A–6B, IMF^{FM}3 to IMF^{FM}14 (last IMF) as well as frequencies greater than 35 Hz in IMF^{FM}1 were removed. For denoising the FM component of *s-signal2*, IMF^{FM}8 to IMF^{FM}13 (last IMF) were removed, as depicted in Fig. 6C–6D.

It should be noted that, as seen in the simulations, to reduce AM component noise in both simulation cases, IMFs^{AM} of frequencies within the range of frequencies with the highest power in the power spectrum are maintained (Figs. 4C and 5C). However, to denoise the FM component of *s-signal2*, only the very low-power IMFs^{FM} are removed as there are multiple peaks in its FM-power spectrum, as shown in Fig. 6C.

Fig. 7 demonstrates the comparison between the pure signal and the resultant signal using the HHSA method and our method for *s-signal1*, and Fig. 8 demonstrates the same comparison for *s-signal2*. The HHSA method produced a signal with modulating frequencies of $\omega = 32.37$ Hz and $\Omega = 3.75$ Hz for *s-signal1*, and results of HHSA application on the noisy signal made of a combination of three career frequencies, *s-signal2*, showed one career frequency $\omega = 45.28$ Hz and $\Omega = 6.83$ Hz.

As shown in Figs. 7 and 8, our proposed method identifies the pure signal's peaks better than the HHSA method. Table I shows the MI computation results for the HHSA and the proposed method applied to *s-signal1* and *s-signal2*.

Simulation	HHSA	Proposed method	Original noisy signal
s-signal1	0.0001	0.3496	0.2991
s-signal2	0.0004	0.4188	0.3564

TABLE I: Comparison of the MI computation results for HHSA and the proposed method applied to *s-signal1* and *s-signal2* with p-value ≤ 0.001.

To show our method's performance on real EEG data (not simulated), we applied the method to a sample of real EEG signal recorded during an EEG-fMRI experiment (see Methods). As shown in Fig. 9, the EEG signal was decomposed into its IMFs applying the ICEEMDAN method [36], with 300 ensembles and a level of noise of 0.2 to have an optimal decomposition of the noisy EEG signal. The frequency spectra of these IMFs corresponded to the EEG frequency bands used in the literature as follows: summation of IMF1 and IMF2 (gamma, > 30 Hz), IMF3 (beta, 12–30 Hz), IMF4 (alpha, 8–12 Hz), IMF5 (theta, 4–8 Hz), and the summation of IMF6 to IMF18 (lambda, 0.1–4 Hz). Fig. 10 shows the result of the application of our method to the gamma band. After constructing the gamma band by summing IMF1 and IMF2 of the real EEG signal, the upper envelope was computed and

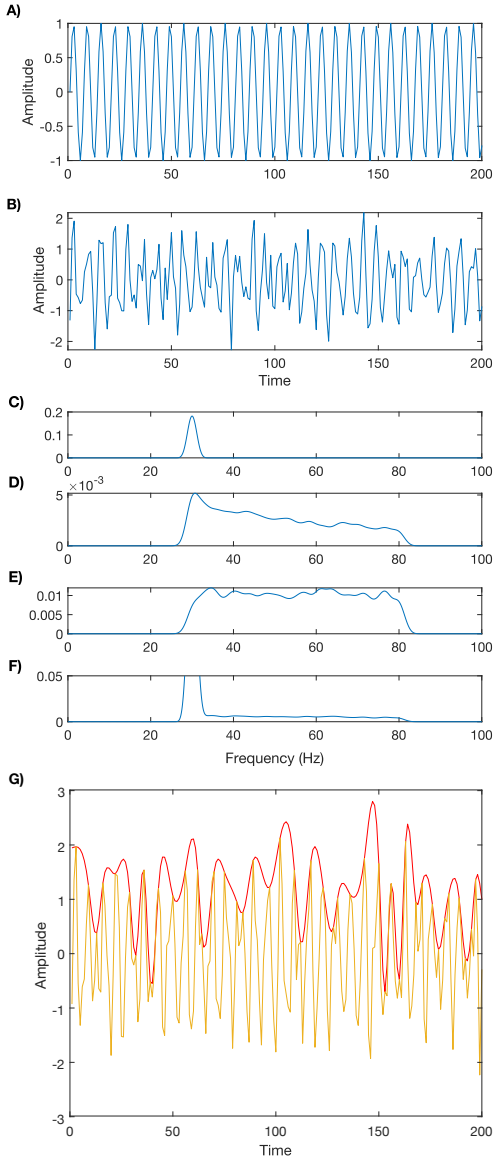

Fig. 2: Representation of the simulated pure and the noisy signal with carrier frequency 30 Hz, their power spectrum and the upper envelope of the simulated noisy signal. A) Simulated pure and B) the noisy signal. 200 time points are shown for illustration purpose. Power spectrum of C) pure signal, D) filtered pink noise, E) filtered white noise, and F) noisy signal. G) Upper envelope of the simulated noisy signal.

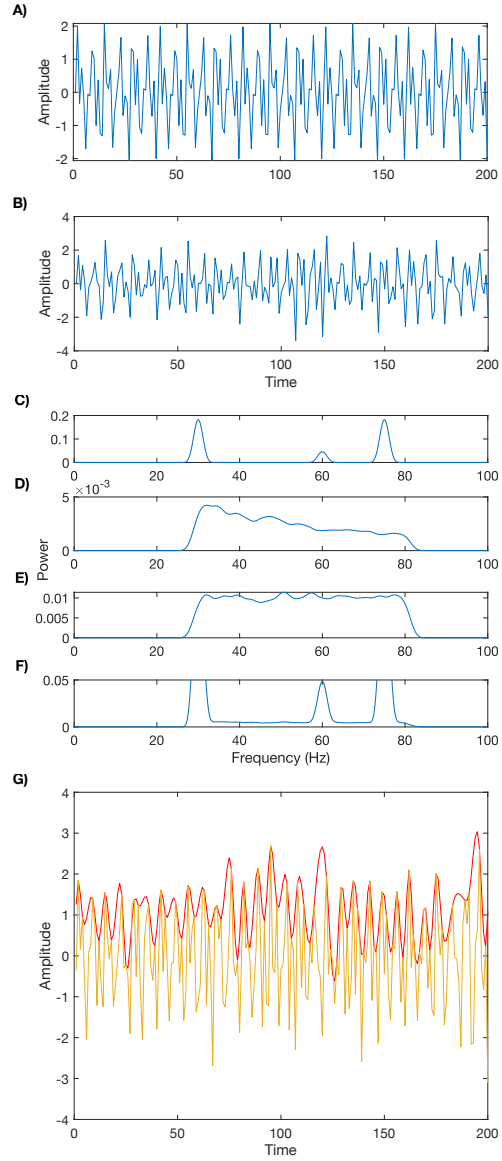

Fig. 3: Representation of the simulated pure and the noisy signal with carrier frequencies of 30, 60, and 70 Hz, their power spectrum and the upper envelope of the simulated noisy signal. A) Simulated pure and B) the noisy signal. 200 time points are shown for illustration purpose. Power spectrum of C) pure signal, D) filtered pink noise, E) filtered white noise, and F) noisy signal. G) Upper envelope of the simulated noisy signal.

decomposed into IMFs^{AM}. Based on the power spectrum of the IMFs^{AM}, the AM components of the gamma signal were denoised by removing IMF^{AM}1 and IMF^{AM}4 to IMF^{AM}10, in which the power intensity was low. Afterwards, the IMFs^{AM} were further denoised by removing frequencies greater than the greatest frequency with a peak in the power spectrum of gamma signal's upper envelope. In this case, frequencies greater than 11 Hz were removed from IMF^{AM}2. On the other hand, the signal's FM portion was denoised by removing IMF^{FM}3 to IMF^{FM}13, as IMF^{FM}1 and IMF^{FM}2 had the greatest power. Furthermore, frequencies greater than 42 Hz were removed from IMF^{FM}1, in accordance with the peak at 42 Hz in the power spectrum of the FM portion of the gamma signal. Fig. 11 compares the power spectral density of the denoised real gamma signal computed by the HHSA and the proposed method. Denoised signal computed by the HHSA method shows almost the same power density as the noisy signal. On the other hand, compared to the HHSA method and the noisy signal, the proposed method shows lower power density in high frequencies of the denoised real gamma signal.

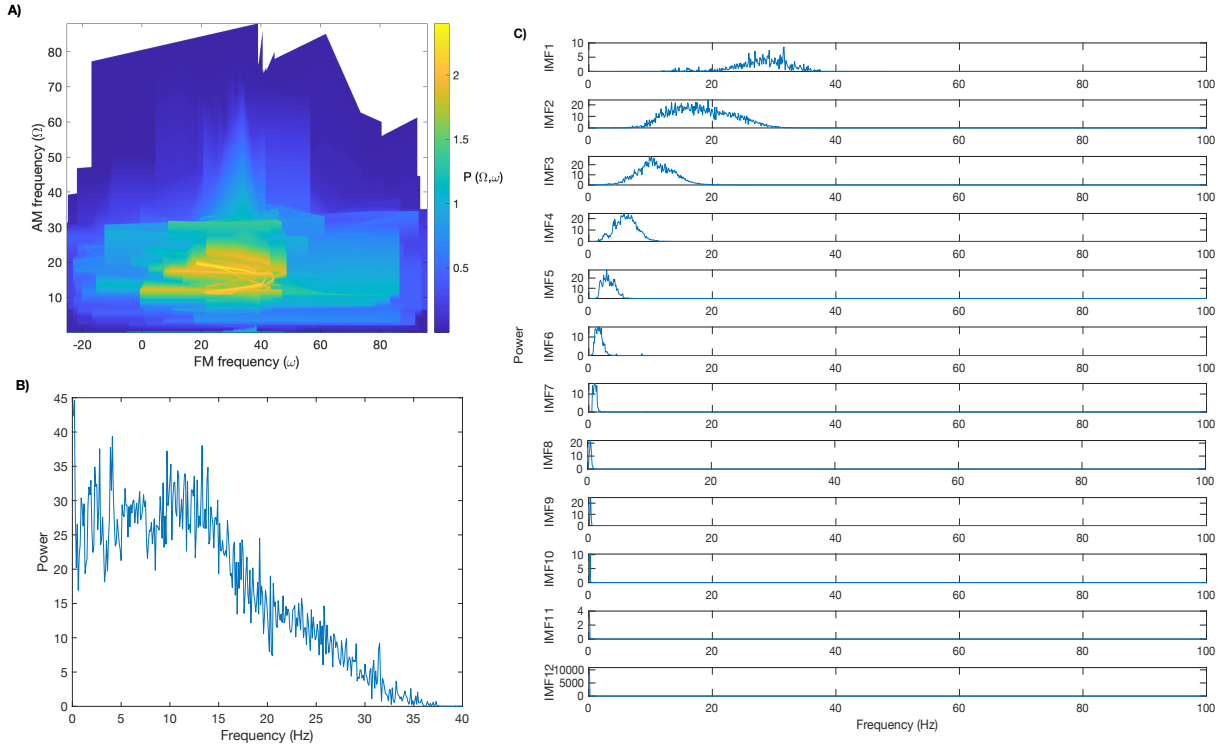

Fig. 4: HHSA spectrum of the noisy signal with carrier frequencies of 30 Hz, its AM power spectrum, and the power spectrum of the IMFs^{AM} of the noisy signal. A) HHSA spectrum of the noisy signal computed using the HHT method, which is based on the instantaneous power and frequencies of all IMFs^{AM} and signal's instantaneous frequencies. B) Power spectra based on the instantaneous frequencies of all IMFs^{AM}. C) Power spectrum of the each of the IMFs^{AM}.

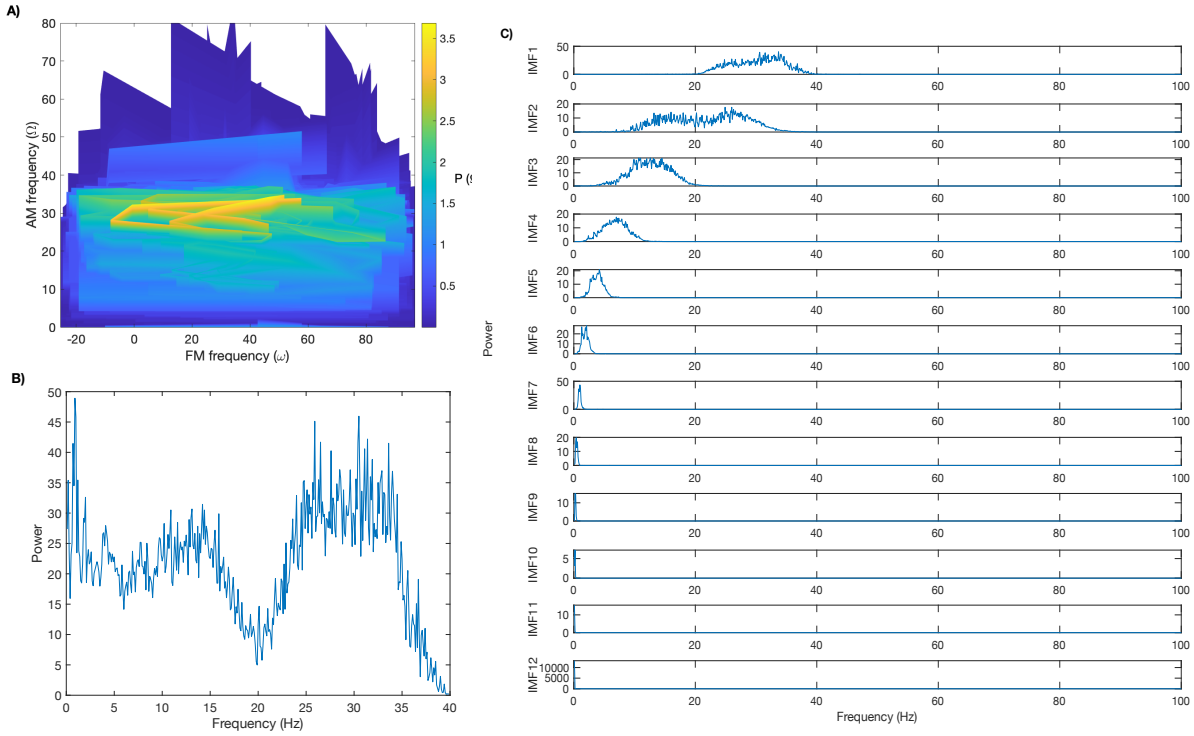

Fig. 5: HHSA spectrum of the noisy signal with combination of three frequencies 30, 60, 75 Hz), its AM power spectrum, and the power spectrum of the IMFs^{AM} of the noisy signal. A) HHSA spectrum of the noisy signal computed by HHT method, which is based on the instantaneous power and frequencies of all IMFs^{AM} and signal's instantaneous frequencies. B) Power spectra based on the instantaneous frequencies of all IMFs^{AM}. C) Power spectrum of the IMFs^{AM}.

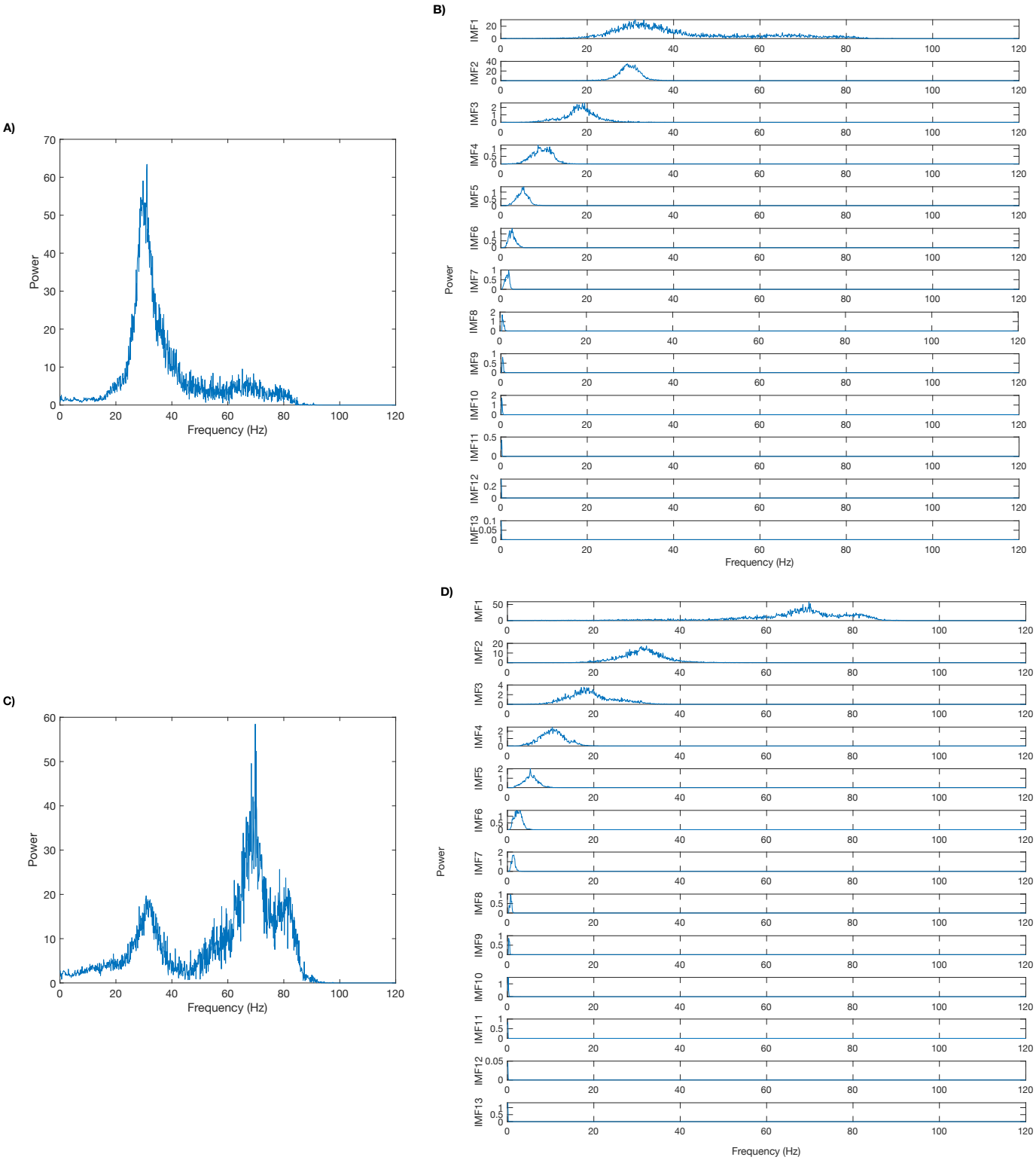

Fig. 6: Power spectrum of the frequency-modulated noisy signals and their IMFs^{FM}. A) and B) are respectively power spectrum of the FM component of 30-Hz signal and its IMFs^{FM}. C) and D) are respectively power spectrum of the FM component of signal with frequencies 30, 60 and 75-Hz, and its IMFs^{FM}.

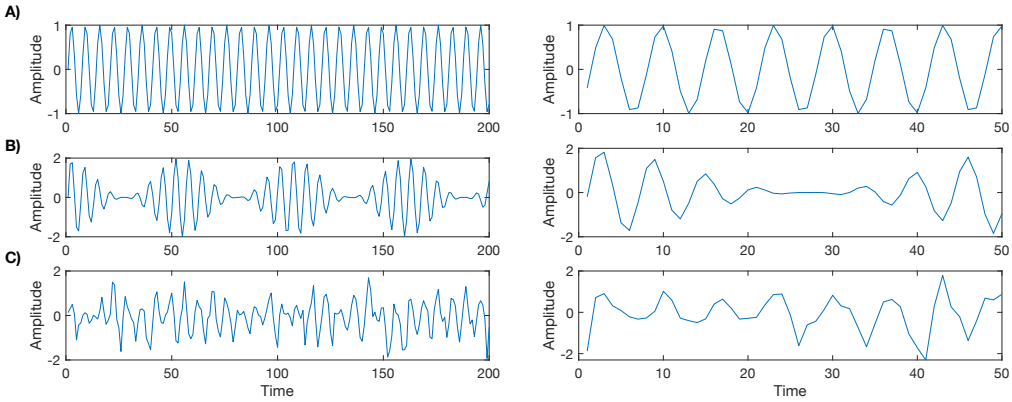

Fig. 7: Comparison between the pure signal with frequency of 30 Hz, the signal denoised using HHSA method, and the signal denoised using the proposed method. 200 time points of the signals are shown for illustration purpose. A) Pure signal. B) Signal with the denoised amplitude based on HHSA method. C) signal with denoised both phase and amplitude using the proposed method. Right panel show 50 time points of each of the signals in the left panel just for illustration purpose.

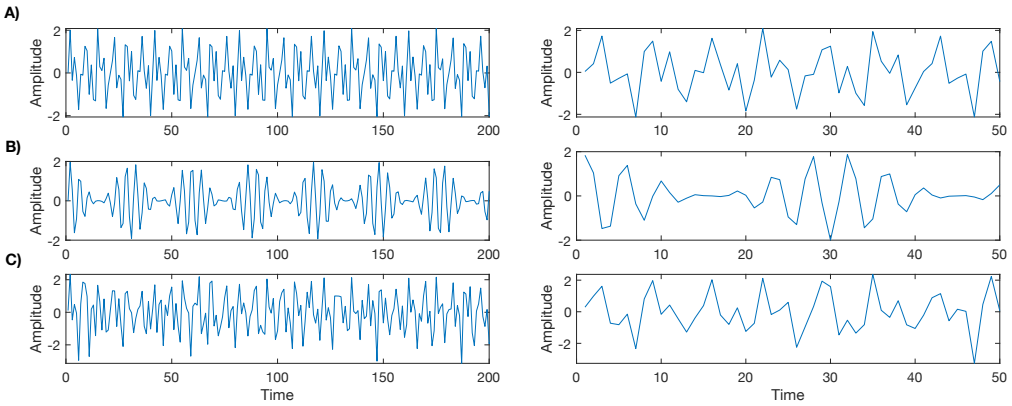

Fig. 8: Comparison between the pure signal, the signal denoised by HHSA method, and the signal denoised by the proposed method when it is made of a combination of 30, 60, and 75 Hz frequencies. 200 time points of the signals are shown for illustration purpose. A) Pure signal. B) Denoised signal by HHSA method. C) Signal with denoised both phase and amplitude by the proposed method. Right panel shows 50 time points of each of the signals in the left panel just for illustration purpose.

IV. Discussion

In this study, Holo-Hilbert based method was used to reduce EEG gamma-band noise. The proposed method denoises any nonstationary and nonlinear time series data; however, the main focus of this paper is gamma-band noise suppression.

Our result showed that when there is more than one peak in the FM-power spectrum of a signal, the HHSA method does not perform as well as when there is a single frequency in each IMFs after the first application of the EMD. In the HHSA method, it is assumed that each IMF computed by the EMD method contains just one frequency; however, this is seldom the case [45, 46], as for example in our second simulated gamma-band signal. Consequently, there might not be a clear discrepancy between peaks in the HHSA spectrum, and we cannot specify separate frequency bands with their specific peak frequencies in the HHSA spectrum. Thus, in these situations, based on the HHSA method, computing the mean frequencies of FM and AM components results in wrong frequencies for the AM and FM components. However, the proposed method does not have this problem as the denoised signal is obtained based on the remaining IMFs after removing IMFs^{AM} and IMFs^{FM} caused by noise. Higher MI for the proposed method compared to the HHSA confirms that the proposed approach extracts the pure signal from the noisy signal with higher efficiency. Moreover, compared to the HHSA method, the proposed method yields lower power density in high frequencies of the denoised real gamma signal which shows its potential to detect and remove problematic artifacts in high-frequency EEG signals.

Furthermore, it is worthy to note that, unlike traditional pre-defined basis methods, e.g., Fourier analysis, wavelet, etc. [8], the AM and the FM components are decomposed separately in the proposed method. Accordingly, AM and FM frequencies are detected separately to reduce the uncertainty of FM frequency detections [6]. Reduction of frequency uncertainty increases the accuracy of a spectral analysis method.

Additionally, the proposed method does not require any reference signal or any assumption on the contaminated EEG data. It can be used on various kinds of data (stationary

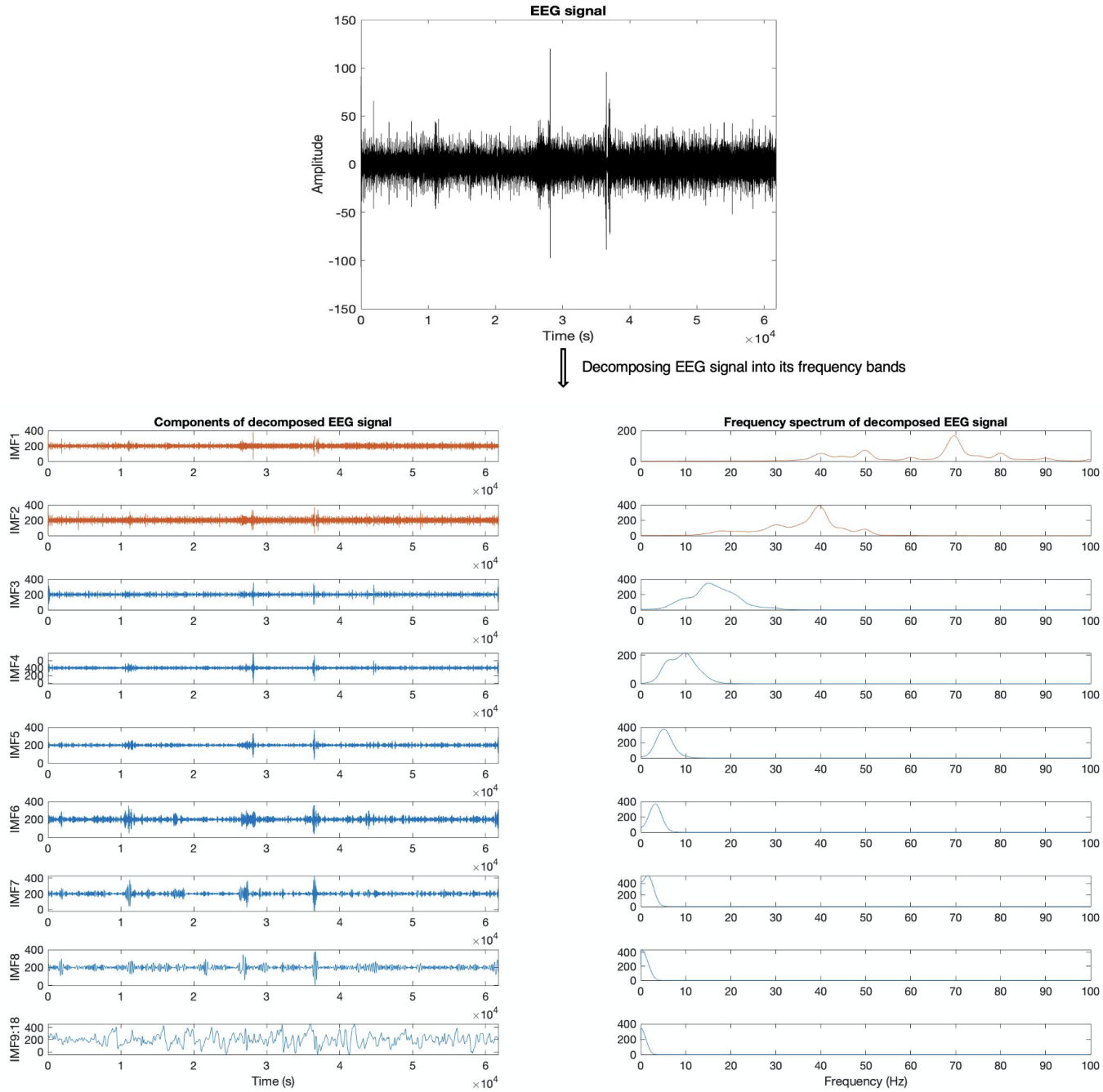

Fig. 9: EEG decomposition into its different bands. A sample of EEG signal is decomposed by applying ICEEMDAN method to specify the gamma band using frequency spectrum. Gamma-band signal is made by the summation of IMF1 and IMF2.

and non-stationary, linear and non-linear) and it suppresses noise with efficacy. However, in this method, the IMFs^{FM} and IMFs^{AM} that should be removed from a signal may vary from subject to subject, and they are specified approximately based on their power spectrum during the noise reduction process. This is also true for choosing the frequencies that should be removed from a specific IMF^{FM}, which is done based on the FM power spectrum. Moreover, the difference in the powers of successive IMFs is sometimes quite small, which makes deciding whether to remove or maintain the subsequent IMF challenging.

Thus, the proposed method acts to effectively reduce noise from the gamma band of EEG by analyzing both the AM and the FM components of the signal. This method applies two layers of EMD to decompose signals adaptively into IMFs with the signal's time-varying amplitude and frequency features. According to the HHSA spectrum and the 2D power spectrums, IMFs^{AM} and IMFs^{FM} (or parts of them) with low powers correspond to noise and are removed from the AM and FM components of the signal. This method will allow for a better realization of neural activity and brain function, especially in studies that use simultaneous EEG and fMRI.

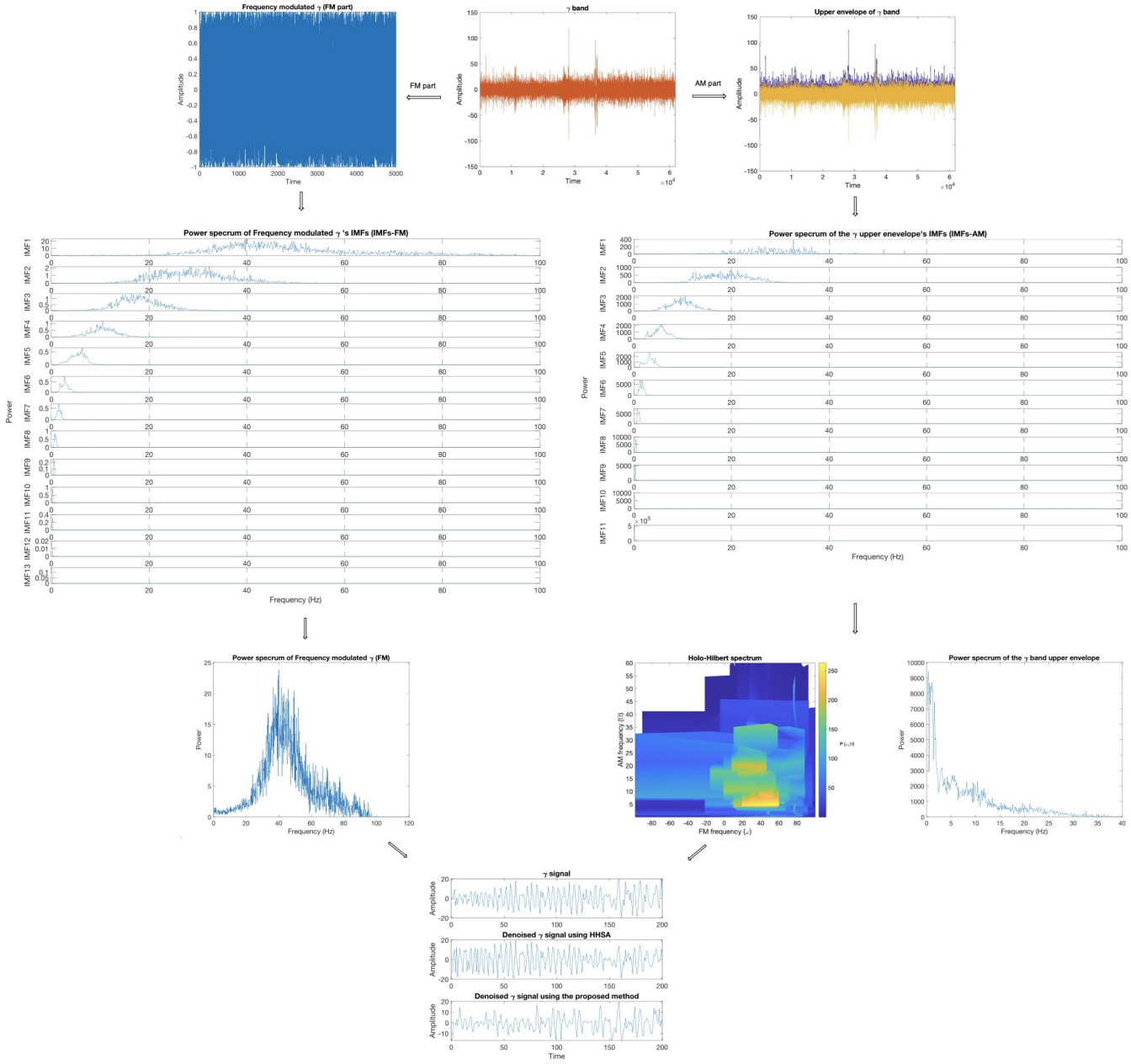

Fig. 10: Pipeline overview of applying the proposed method to denoise the FM and AM components of the real gamma band. Steps of applying the proposed method to the gamma-band signal are as follow: 1) Computing the upper envelope of the gamma signal and the frequency modulated gamma signal. 2) Computing the power spectrum of the decomposed AM and the FM components (IMFs^{AM} and IMFs^{FM}). 3) Computing the power spectrum of the AM and FM parts. 4) Denoising the upper envelope using Holo-Hilbert spectrum by removing $\text{IMF}^{\text{AM}}1$ and $\text{IMF}^{\text{AM}}4$ to $\text{IMF}^{\text{AM}}10$ and also removing frequency higher than 11 Hz from $\text{IMF}^{\text{AM}}2$ based on the power spectrum of the gamma signal's upper envelope. FM part of the signal was denoised by removing $\text{IMF}^{\text{FM}}3$ to $\text{IMF}^{\text{FM}}13$. Furthermore, frequencies higher than 42 Hz were removed from $\text{IMF}^{\text{FM}}1$. 5) Comparing the noisy gamma signals with its different denoised versions.

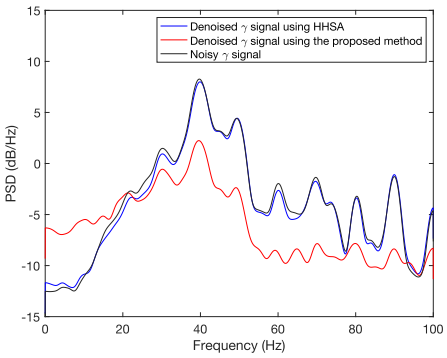

Fig. 11: Comparison of the power spectrum density for the HHSA and the proposed method applied to the sample real gamma signal.

Authors' Contribution

NM and RS designed the research. NM simulated and analyzed the data, interpreted the results and wrote the manuscript. PL acquired and preprocessed real EEG data and helped with manuscript evaluation. BA acquired and preprocessed real EEG data. BG helped with data interpretation and manuscript evaluation. RS supervised the development of the work, helped with data interpretation and manuscript evaluation.

Funding Statement

This work was supported by grant RGPIN-2015-05966 from Natural Sciences and Engineering Research Council of Canada.

References

[1] A. M. Dale et al., "Dynamic statistical parametric mapping: combining fMRI and MEG for high-resolution imaging of cortical activity," Neuron, vol. 26, no. 1, pp. 55–67, Apr 2000.

[2] D. L. Schomer, "Niedermeyer's Electroencephalography: Basic Principles, Clinical Applications, and Related Fields ", F. H. L. d. Silva, Ed., ed: Oxford University Press, 2017.

[3] R. Buxton, Introduction to Functional Magnetic Resonance Imaging: Principles and Techniques (2nd ed.). Cambridge:: Cambridge University Press, 2009.

[4] K. Whittingstall and N. K. Logothetis, "Frequency-band coupling in surface EEG reflects spiking activity in monkey visual cortex," Neuron, vol. 64, no. 2, pp. 281–289, Oct 29 2009.

[5] J. R. Ives, S. Warach, F. Schmitt, R. R. Edelman, and D. L. Schomer, "Monitoring the patient's EEG during echo planar MRI," Electroencephalogr Clin Neurophysiol, vol. 87, no. 6, pp. 417–20, Dec 1993.

[6] H. T. Hsu, W. K. Lee, K. K. Shyu, T. K. Yeh, C. Y. Chang, and P. L. Lee, "Analyses of EEG Oscillatory Activities During Slow and Fast Repetitive Movements Using Holo-Hilbert Spectral Analysis," Ieee T Neur Sys Reh, vol. 26, no. 9, pp. 1659–1668, Sep 2018.

[7] R. J. Huster, S. Debener, T. Eichele, and C. S. Herrmann, "Methods for Simultaneous EEG-fMRI: An Introductory Review," J Neurosci, vol. 32, no. 18, pp. 6053-6060, May 2 2012.

[8] N. K. Logothetis, "What we can do and what we cannot do with fMRI," Nature, vol. 453, no. 7197, pp. 869-78, Jun 12 2008.

[9] R. Scheeringa et al., "Neuronal dynamics underlying high- and low-frequency EEG oscillations contribute independently to the human BOLD signal," Neuron, vol. 69, no. 3, pp. 572–83, Feb 10 2011.

[10] Y. Murayama et al., "Relationship between neural and hemodynamic signals during spontaneous activity studied with temporal kernel CCA," Magn Reson Imaging, vol. 28, no. 8, pp. 1095–1103, Oct 2010.

[11] M. D. Fox and M. E. Raichle, "Spontaneous fluctuations in brain activity observed with functional magnetic resonance imaging," Nat Rev Neurosci, vol. 8, no. 9, pp. 700–11, Sep 2007.

[12] S. Harris et al., "Coupling between gamma-band power and cerebral blood volume during recurrent acute neocortical seizures," Neuroimage, vol. 97, pp. 62–70, Aug 2014.

[13] A. Shmuel and D. A. Leopold, "Neuronal correlates of spontaneous fluctuations in fMRI signals in monkey visual cortex: Implications for functional connectivity at rest," Hum Brain Mapp, vol. 29, no. 7, pp. 751–61, Jul 2008.

[14] J. P. Lachaux et al., "Relationship between task-related gamma oscillations and BOLD signal: new insights from combined fMRI and intracranial EEG," Hum Brain Mapp, vol. 28, no. 12, pp. 1368–75, Dec 2007.

[15] A. Brovelli, J. P. Lachaux, P. Kahane, and D. Boussaoud, "High gamma frequency oscillatory activity dissociates attention from intention in the human premotor cortex," Neuroimage, vol. 28, no. 1, pp. 154–64, Oct 2005.

[16] C. a. L. L. Mulert, EEG-fMRI: physiological basis, technique, and applications. Springer Science & Business Media, 2009.

[17] N. K. Logothetis, J. Pauls, M. Augath, T. Trinath, and A. Oeltermann, "Neurophysiological investigation of the basis of the fMRI signal," Nature, vol. 412, no. 6843, pp. 150–157, Jul 2001.

[18] E. Basar, C. Basar-Eroglu, S. Karakas, and M. Schurmann, "Brain oscillations in perception and memory," Int J Psychophysiol, vol. 35, no. 2-3, pp. 95–124, Mar 2000.

[19] A. von Stein and J. Sarnthein, "Different frequencies for different scales of cortical integration: from local gamma to long range alpha/theta synchronization," Int J Psychophysiol, vol. 38, no. 3, pp. 301–13, Dec 1 2000.

[20] D. A. Leopold, Y. Murayama, and N. K. Logothetis, "Very slow activity fluctuations in monkey visual cortex: implications for functional brain imaging," Cereb Cortex, vol. 13, no. 4, pp. 422–33, Apr 2003.

[21] D. Mantini, M. G. Perrucci, C. Del Gratta, G. L. Romani, and M. Corbetta, "Electrophysiological signatures of resting state networks in the human brain," Proc Natl Acad Sci U S A, vol. 104, no. 32, pp. 13170-5, Aug 2007.

[22] R. K. Niazy, C. F. Beckmann, G. D. Iannetti, J. M. Brady, and S. M. Smith, "Removal of FMRI environment artifacts from EEG data using optimal basis sets," Neuroimage, vol. 28, no. 3, pp. 720–737, Nov 15 2005.

[23] J. L. Ferreira, Y. Wu, R. M. Besseling, R. Lamerichs, and R. M. Aarts, "Gradient Artefact Correction and Evaluation of the EEG Recorded Simultaneously with fMRI Data Using Optimised Moving-Average," J Med Eng, vol. 2016, p. 9614323, 2016.

[24] L. Sun and H. Hinrichs, "Simultaneously recorded EEG-fMRI: removal of gradient artifacts by subtraction of head movement related average artifact waveforms," Hum Brain Mapp, vol. 30, no. 10, pp. 3361–77, Oct 2009.

[25] I. Kaya, "A Brief Summary of EEG Artifact Handling," arXiv preprint arXiv:2001.00693., 2019.

[26] C. K. Chui, Chen, G., "Kalman filtering: with real-time applications," Springer Series in Information Sciences, vol. 17, Springer, Berlin, vol. 17, 1999.

[27] I. Daubechies, "Wavelets - Algorithms and Applications - Meyer,Y,", Science, vol. 262, no. 5139, pp. 1589–1591, Dec 3 1993.

[28] P. Comon, and Jutten, C., "Handbook of Blind Source Separation, Independent Component Analysis and Applications," 1st Edn. Boston, MA: Academic Press; Elsevier., 2010.

[29] N. Hoogenboom, J. M. Schoffelen, R. Oostenveld, L. M. Parkes, and P. Fries, "Localizing human visual gamma-band activity in frequency, time and space," Neuroimage, vol. 29, no. 3, pp. 764–773, Feb 1 2006.

[30] P. Anderer et al., "Artifact processing in computerized analysis of sleep EEG - A review," Neuropsychobiology, vol. 40, no. 3, pp. 150–157, 1999.

[31] D. J. McFarland, L. M. McCane, S. V. David, and J. R. Wolpaw, "Spatial filter selection for EEG-based communication," Electroen Clin Neuro, vol. 103, no. 3, pp. 386–394, Sep 1997.

[32] P. J. Allen, O. Josephs, and R. Turner, "A method for removing imaging artifact from continuous EEG recorded during functional MRI," Neuroimage, vol. 12, no. 2, pp. 230–239, Aug 2000.

[33] N. E. Huang et al., "On Holo-Hilbert spectral analysis: a full informational spectral representation for nonlinear and non-stationary data," Philos Trans A Math Phys Eng Sci, vol. 374, no. 2065, p. 20150206, Apr 13 2016.

[34] N. E. Huang, "Introduction to the Hilbert-Huang transform and its related mathematical problems," Interd Math Sci, vol. 5, pp. 1–26, 2005.

[35] N. E. Huang et al., "The empirical mode decomposition and the Hilbert spectrum for nonlinear and non-stationary time series analysis," P Roy Soc a-Math Phy, vol. 454, no. 1971, pp. 903–995, Mar 8 1998.

[36] M. A. Colominas, G. Schlotthauer, and M. E. Torres, "Improved complete ensemble EMD: A suitable tool for biomedical signal processing," Biomed Signal Proces, vol. 14, pp. 19–29, Nov 2014.

[37] K. T. Nguyen et al., "Unraveling nonlinear electrophysiologic processes in the human visual system with full dimension spectral analysis," Sci Rep, vol. 9, no. 1, p. 16919, 11 2019.

[38] A. C. Nobre and F. van Ede, "Under the Mind's Hood: What We Have Learned by Watching the Brain at Work," J Neurosci, vol. 40, no. 1, pp. 89–100, 01 2020.

[39] Y. L. Liangjie Wei, Jing Wang, Yan Ma, "Time-Frequency Convolutional Neural Network for Automatic Sleep Stage Classification Based on Single-Channel EEG," ed: 2017 International Conference on Tools with Artificial Intelligence, 2017.

[40] S. Y. Zhang, J. Hennig, and P. LeVan, "Direct modelling of gradient artifacts for EEG-fMRI denoising and motion tracking," J Neural Eng, vol. 16, no. 5, Oct 2019.

[41] P. LeVan, J. Maclaren, M. Herbst, R. Sostheim, M. Zaitsev, and J. Hennig, "Ballistocardiographic artifact removal from simultaneous EEG-fMRI using an optical motion-tracking system," Neuroimage, vol. 75, pp. 1–11, Jul 15 2013.

[42] P. LeVan, S. Zhang, B. Knowles, M. Zaitsev, and J. Hennig, "EEG-fMRI Gradient Artifact Correction by Multiple Motion-Related Templates," IEEE Trans Biomed Eng, vol. 63, no. 12, pp. 2647–2653, 12 2016.

[43] M. O'Sullivan, A. Temko, A. Bocchino, C. O'Mahony, G. Boylan, and E. Popovici, "Analysis of a Low-Cost EEG Monitoring System and Dry Electrodes toward Clinical Use in the Neonatal ICU," Sensors-Basel, vol. 19, no. 11, Jun 1 2019.

[44] D. M. Goldenholz et al., "Mapping the signal-to-noise-ratios of cortical sources in magnetoencephalography and electroencephalography," Hum Brain Mapp, vol. 30, no. 4, pp. 1077–86, Apr 2009.

[45] G. Rilling, "One or two frequencies? The empirical mode decomposition answers," vol. 56, P. Flandrin, Ed., ed: IEEE Trans. Signal Process., 2008, p. 8595.

[46] S.-S. Lu, "An EMD-based principal frequency analysis with applications to nonlinear mechanics," Mechanical Systems and Signal Processing, vol. 150, 2021.

[47] U. Melia et al., "Prediction of Nociceptive Responses during Sedation by Linear and Non-Linear Measures of EEG Signals in High Frequencies," Plos One, vol. 10, no. 4, Apr 22 2015.